Surgical and Radiologic Anatomy (2019) 41:551–567
https://doi.org/10.1007/s00276-019-02179-x

ORIGINAL ARTICLE

Morphometric evaluation and clinical implications of the greater palatine foramen, greater palatine canal and pterygopalatine fossa on CBCT images and review of literature

İlhan Bahşi[1] · Mustafa Orhan[1] · Piraye Kervancıoğlu[1] · Eda Didem Yalçın[2]

Received: 1 August 2018 / Accepted: 3 January 2019 / Published online: 8 January 2019

Abstract

Introduction The pterygopalatine fossa (PPF) infiltration is performed to reduce blood flow during endoscopic sinus surgery and septorhinoplasty, as well as to control posterior epistaxis and provide regional anesthesia in dental procedures. PPF infiltration performed with consideration of the morphometrics of greater palatine foramen (GPF), greater palatine canal (GPC) and PPF would increase the success of the procedure and reduce the risk of complications. The aim of this study is to investigate the GPF, GPC, lesser palatine foramen (LPF), lesser palatine canal (LPC) and PPF morphology via the images obtained by CBCT, to provide information for interventional procedures.

Materials and methods GPF, GPC, LPF, LPC and PPF were morphometrically evaluated retrospectively in CBCT images of 75 female and 75 male cases by Planmeca Romexis program. The 19 parameters were measured on these images.

Results These parameters were evaluated statistically. The comparison of these parameters by genders revealed significant differences in distances between GPC–PC, PC–IOF, LPC–GPF, GPF–MS in the coronal and transverse planes, the distance between GPF and the occlusal plane of the teeth, GPF–PNS, GPF–IF and TD-GPF, and in the area of GPF. The number of LPF was found ranging from 1 to 5.

Conclusion Our results may help to insert to needle properly for application of maxillary nerve block with a high success rate and minimal complication. We recommend that the needle should be inserted 14–15 mm lateral to the midsagittal plane, 19–20 mm over the occlusal plane of the teeth and on the same line with the third molar teeth. For PPF infiltration through the GPF, the needle should be pushed forward 28 mm upward at 66° angle on the transverse plane and 14°–15° angle on the vertical plane.

Keywords Greater palatine canal · Greater palatine foramen · Lesser palatine canal · Lesser palatine foramen · Pterygopalatine fossa · Cone-beam computed tomography · Maxillary nerve block

Abbreviations

AR	Alveolar ridge
GPC	Greater palatine canal
GPF	Greater palatine foramen
IF	Incisive foramen
IOF	Inferior orbital fissure
LPC	Lesser palatine canal
LPF	Lesser palatine foramen
MS	Midsagittal plane
PC	Pterygoid canal
PH	Pterygoid hamulus
PNS	Posterior nasal spine
PPF	Pterygopalatine fossa
TP	Transverse plane
VP	Vertical plane

✉ İlhan Bahşi
dr.ilhanbahsi@gmail.com

Mustafa Orhan
mustafarhn@yahoo.com

Piraye Kervancıoğlu
pirayek@hotmail.com

Eda Didem Yalçın
didemyalcn@gmail.com

[1] Department of Anatomy, Faculty of Medicine, Gaziantep University, Gaziantep, Turkey

[2] Department of Dentomaxillofacial Radiology, Faculty of Dentistry, Gaziantep University, Gaziantep, Turkey

Introduction

The pterygopalatine fossa (PPF) is an inverted pyramid-shaped space located on the side of the skull in the medial aspect of the infratemporal fossa. It is connected with the middle cranial fossa via the round foramen and pterygoid canal (PC) (Vidian canal) posteriorly, with the orbit via the inferior orbital fissure (IOF) superiorly, with the nasal cavity via the sphenopalatine foramen medially, with the infratemporal fossa via the pterygomaxillary fissure laterally and with the oral cavity via the greater palatine canal (GPC) inferiorly [44, 53]. Within the PPF, there are maxillary artery, vein, nerve and their branches, as well as the pterygopalatine ganglion. The greater palatine nerve leaving the pterygopalatine ganglion within the PPF passes through the GPC and emerges to the greater palatine foramen (GPF) in the hard palate. The greater palatine nerve branches to the lesser palatine nerves within the GPC. The lesser palatine nerves descend through the lesser palatine canals (LPCs) and emerge in the hard palate via the lesser palatine foramina (LPFs) [8, 44].

Anesthetic solutions for the regional anesthesia and the vasoconstrictor solutions against bleeding during endoscopic sinus surgery and septorhinoplasty, as well as for helping control posterior epistaxis, can be administered into the PPF through the GPC [13, 20, 57]. It has been reported that PPF infiltration through the GPC may lead to complications such as insufficient anesthesia, blood aspiration, trauma of palatine nerves, intravascular injection, diplopia, strabismus and ptosis [13, 47]. A PPF infiltration performed with consideration of the morphometrics of GPF, GPC and PPF would increase the success of the procedure and reduce the risk of complications.

The aim of this study is to investigate the PPF, GPC, LPC, GPF and LPF morphology via the images obtained by cone-beam computed tomography (CBCT), to provide information for interventional procedures.

Materials and methods

Permission was obtained from the Clinical Trials Ethics Committee before the study commenced. A total of 150 cone-beam computed tomography images with no pathology of 75 female and 75 male subjects aged 18–65 years were selected randomly. The images of patients who were admitted to Gaziantep University Faculty of Dentistry for any reason were evaluated retrospectively by Planmeca Romexis (Planmeca, Helsinki, Finland) program. The following were excluded from the study: the CBCT images of the subjects with any missing or conflicting sections, an artifact image that impairs the detection or measurement of the reference points, pathologies that may affect the sizes of the PPF and the GPC. GPF, LPF, GPC, LPC and PPF of the cases were bilaterally (300 sides of 150 cases) examined. The following 19 parameters were measured on these images in sagittal, coronal and axial planes.

The parameters were measured in the sagittal planes:

1. The distance between the GPF and the PC (GPF–PC) (Fig. 1a).

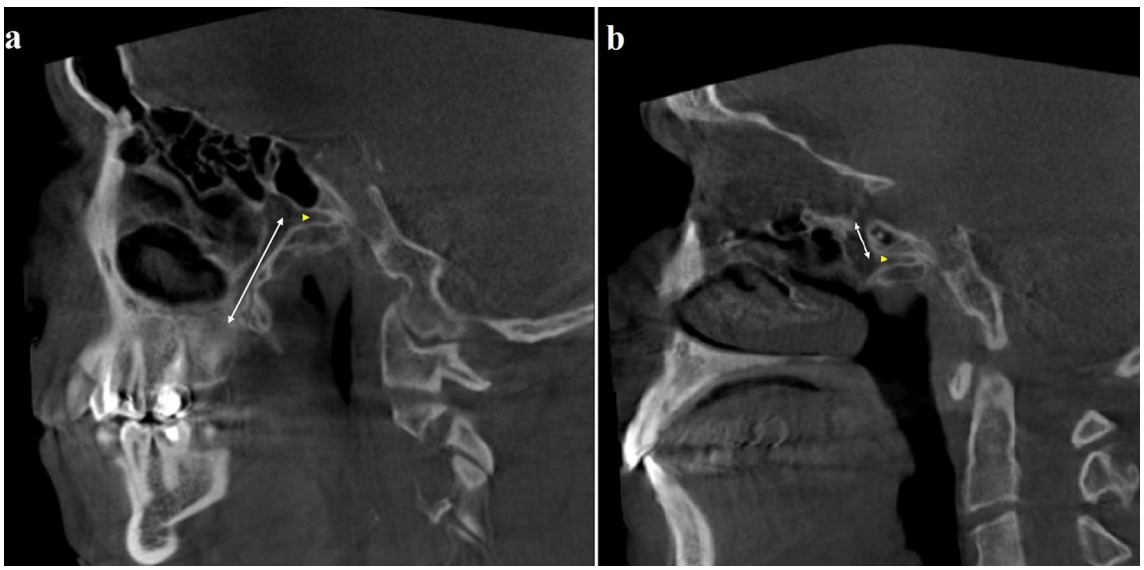

Fig. 1 The distance between the GPF and the PC (**a**), and the distance between the PC and the IOF (**b**) (yellow arrow: pterygoid canal). *GPF* greater palatine foramen, *IOF* inferior orbital fissure, *PC* pterygoid canal

2. The distance between the PC and the IOF (PC–IOF) (Fig. 1b).
3. The distance between the beginning of the LPC and the GPF (LPC–GPF) (Fig. 2).
4. The angle between the axis of the GPC and the axis of the PPF (Fig. 3a).
5. The angle between the transverse plane and the axis of the GPC (TP–GPC) (Fig. 3b).

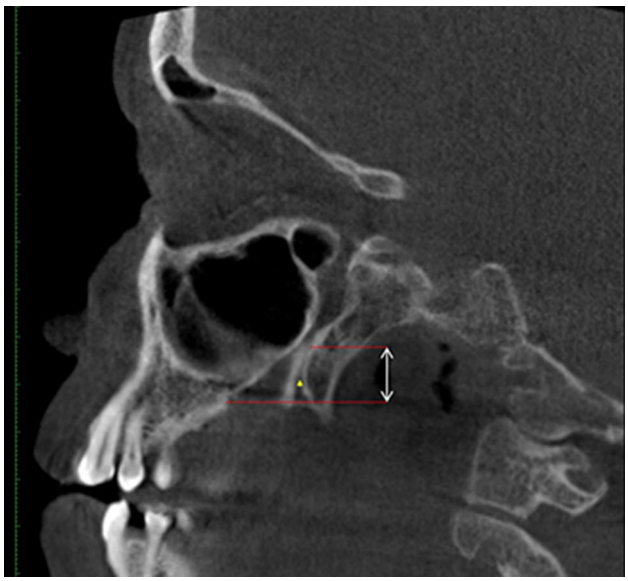

Fig. 2 The distance between the beginning of the LPC and the GPF (yellow arrow: LPC). *GPF* greater palatine foramen, *LPC* lesser palatine canal

The following parameters were measured in the coronal planes:

6. The distance between the GPF and the midsagittal plane (GPF–MS) (Fig. 4a).
7. The distance between the GPF and the occlusal plane of the teeth (Fig. 4b).
8. The angle between the vertical plane and the axis of the GPC (VP–GPC) (Fig. 4c).

The parameters were measured in the axial planes:

9. The transverse diameter of the GPF (TD-GPF) (Fig. 5a).
10. The sagittal diameter of the GPF (SD-GPF) (Fig. 5b).
11. The area of the GPF (Fig. 5c).
12. The distance between the GPF and midsagittal plane (GPF–MS) (Fig. 5d).
13. The distance between the GPF and the posterior nasal spine (GPF–PNS) (Fig. 6a).
14. The distance between the GPF and the incisive foramen (GPF–IF) (Fig. 6b).
15. The distance between the GPF and the pterygoid hamulus (GPF–PH) (Fig. 6c).
16. The distance between the GPF and the alveolar ridge (GPF–AR)
17. The number of LPF (Fig. 7).
18. The localization of the GPF with respect to the posterior margin of the palatine bone (Fig. 8).
19. The localization of the GPF according to the maxillary molar teeth.

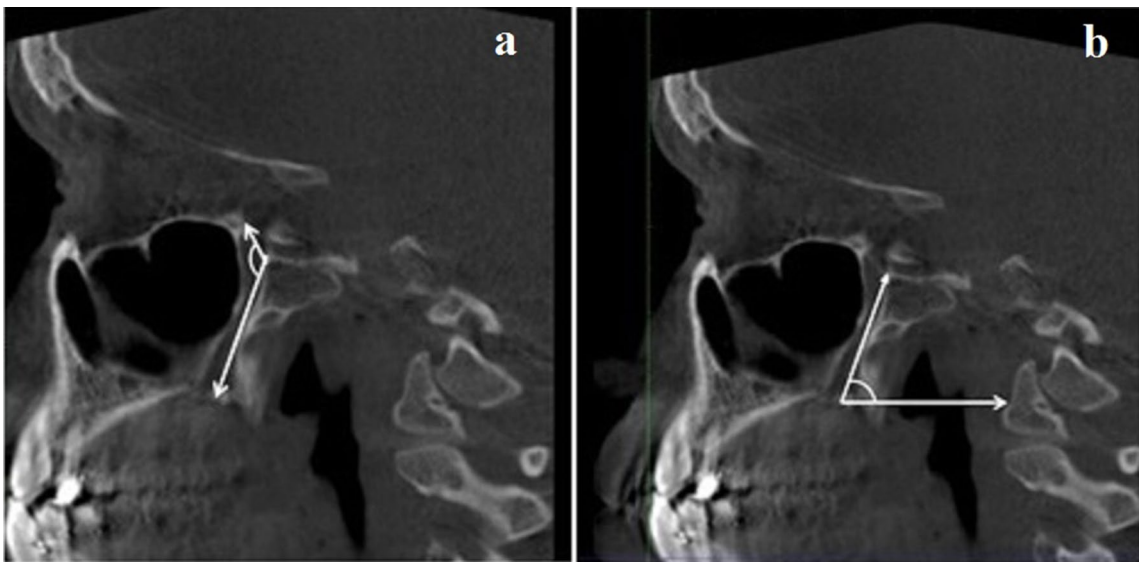

Fig. 3 The angle between the axis of the GPC and the axis of the PPF (**a**), and the angle between the transverse plane and the axis of the GPC (**b**). *GPC* greater palatine canal, *PPF* pterygopalatine fossa

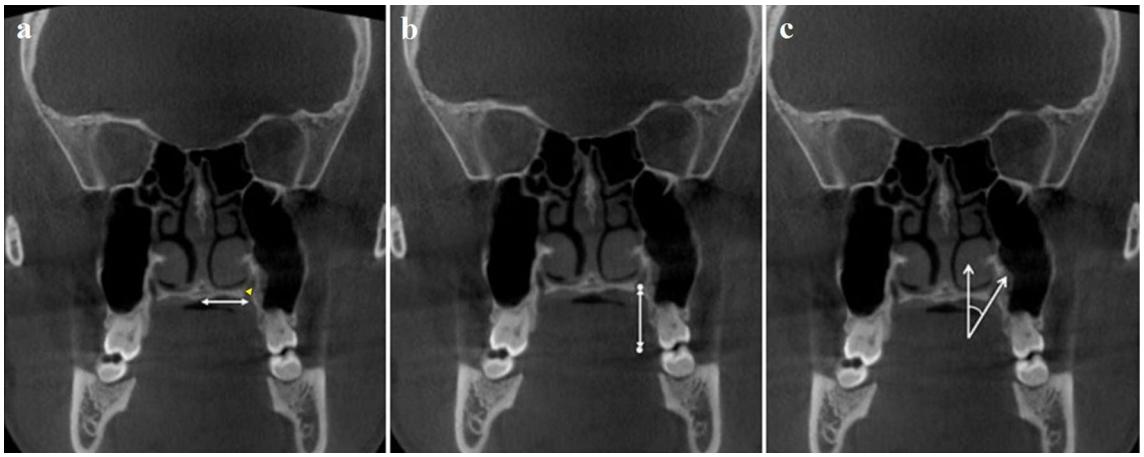

Fig. 4 The distance between the GPF and the midsagittal plane (**a**), the distance between the GPF and the occlusal plane of the teeth (**b**) and the angle between the vertical plane and the axis of the GPC (**c**) (yellow arrow: GPC). *GPF* greater palatine foramen

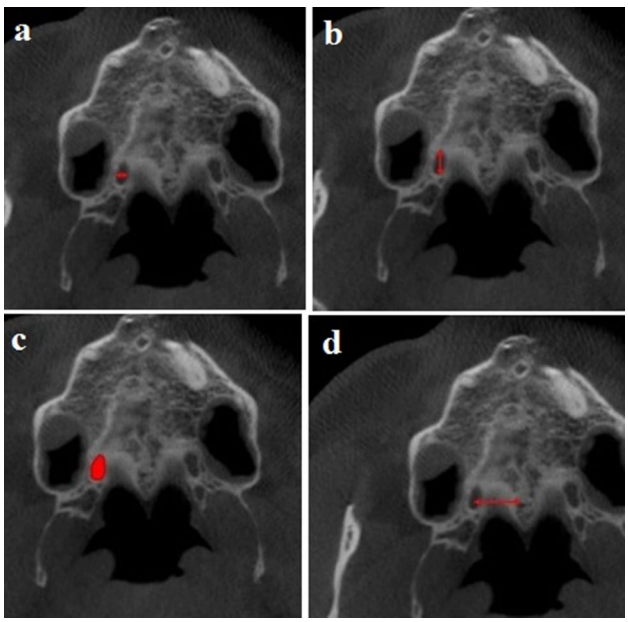

Fig. 5 The transverse diameter of the GPF (**a**), the sagittal diameter of the GPF (**b**), the area of the GPF (**c**) and the distance between the GPF and the midsagittal plane (**d**). *GPF* greater palatine foramen

The data were statistically evaluated. The suitability of the data for normal distribution was tested using the Shapiro–Wilk test. The Student's *t* test was used to compare normally distributed variables in two independent groups, while paired samples *t* test was used to compare two dependent measurements. The Pearson correlation coefficient was used to test the relationships among numerical variables. The SPSS 22.0 software package was used in the analyses. $p < 0.05$ was accepted as being statistically significant.

Results

In this study, PPF, GPC, LPC, GPF and LPF were morphometrically evaluated bilaterally in CBCT images of 75 female and 75 male cases with a range of 18–65 years (*F*: 39.77 ± 13.96, *M*: 40.35 ± 12.84). No significant age difference existed between genders ($p > 0.711$). The values of the parameters by gender and side are presented in Table 1.

The comparison of these parameters by genders revealed significant differences in distances between *GPC–PC* ($p = 0.001$), *PC–IOF* ($p = 0.001$), *LPC–GPF* ($p = 0.001$),

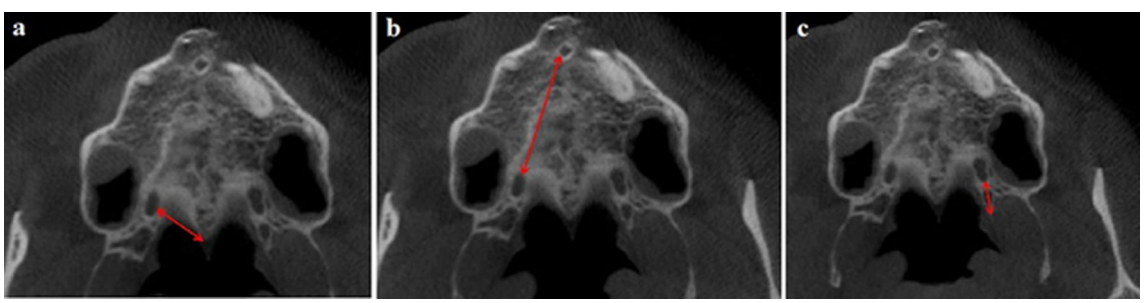

Fig. 6 The distance between the GPF and the posterior nasal spine (**a**), the distance between the GPF and the incisive foramen (**b**) and the distance between the GPF and the pterygoid hamulus (**c**). *GPF* greater palatine foramen

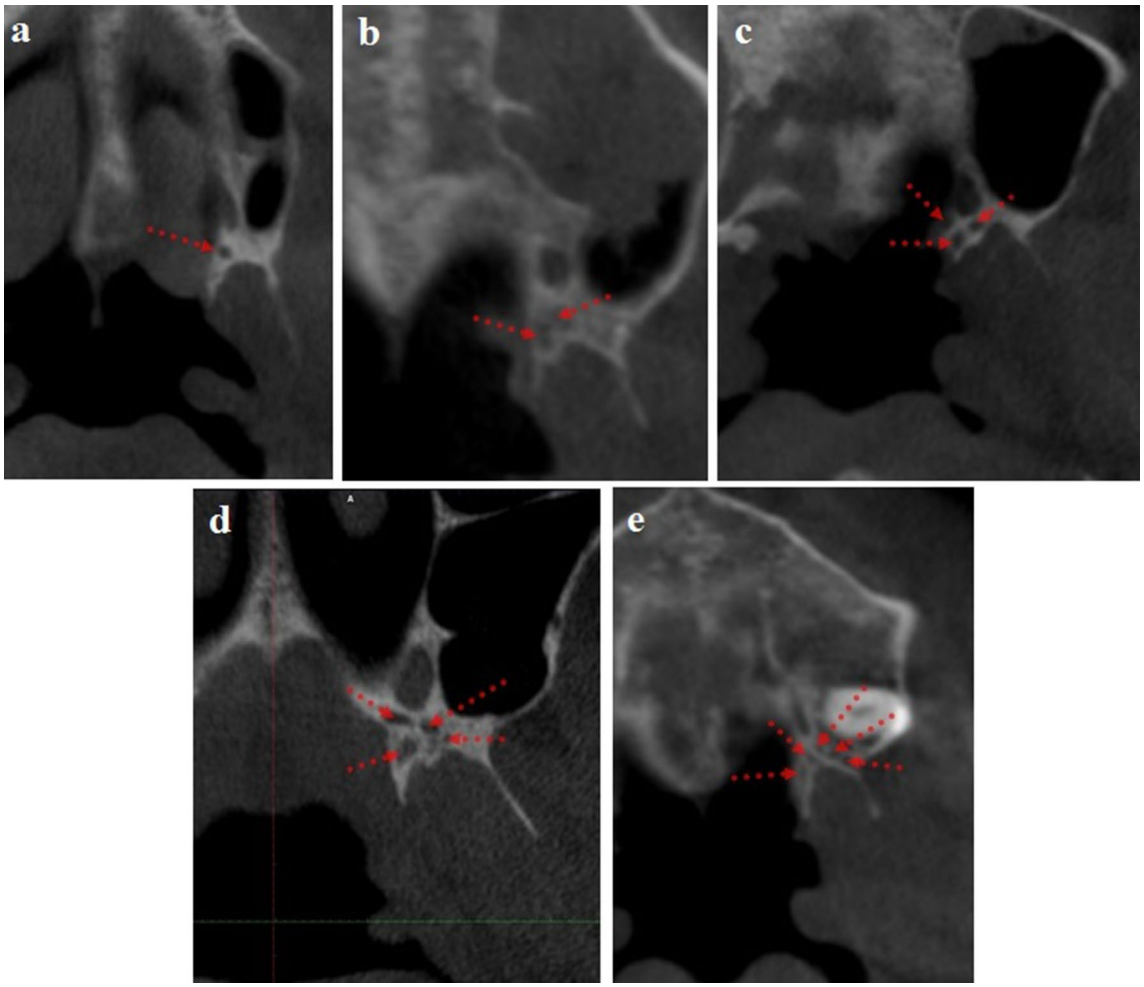

Fig. 7 The number of the LPF (**a** one, **b** two, **c** three, **d** four, **e** five). *LPF* lesser palatine foramen

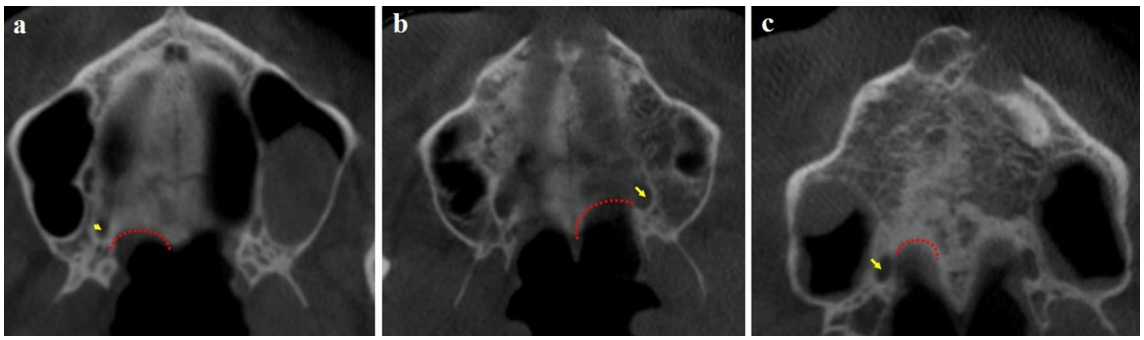

Fig. 8 The localization of the GPF with respect to the posterior margin of the palatine bone (**a** anteriorly, **b** on the same line, **c** posteriorly) (yellow arrow: GPF). *GPF* greater palatine foramen

GPF–MS in the coronal plane ($p = 0.001$), *GPF–MS* in the transverse plane ($p = 0.041$), the distance between GPF and the occlusal plane of the teeth ($p = 0.001$), *GPF–PNS* (0.001), *GPF–IF* ($p = 0.001$) and *TD-GPF* ($p = 0.001$), and in the area of GPF ($p = 0.001$).

In this study, the number of LPF was found ranging from 1 to 5 (Fig. 7a–e). The number of LPF by gender and side

Table 1 The measurements of parameters

	Parameter	G	Right	Left	*p*
1	GPF–PC (mm)	F	27.48 ± 3.10	26.71 ± 2.82	0.039*
		M	29.27 ± 3.59	29.33 ± 3.14	0.869
		T	28.37 ± 3.46	28.02 ± 3.25	0.203
2	PC–IOF (mm)	F	8.34 ± 2.51	8.68 ± 2.43	0.367
		M	9.55 ± 2.93	9.42 ± 2.43	0.709
		T	8.95 ± 2.78	9.04 ± 2.45	0.667
3	LPC–GPF (mm)	F	12.44 ± 2.69	12.88 ± 2.59	0.370
		M	13.78 ± 3.07	13.96 ± 3.37	0.724
		T	13.17 ± 2.90	13.39 ± 3.03	0.388
4	The angle between the axis of the GPC and the axis of the PPF (°)	F	150.82 ± 8.97	151.85 ± 9.34	0.328
		M	149.43 ± 9.88	150.41 ± 8.87	0.389
		T	150.12 ± 9.42	151.13 ± 9.11	0.192
5	The angle between the transverse plane and the axis of the GPC (°)	F	66.13 ± 6.59	65.81 ± 5.42	0.638
		M	65.74 ± 7.03	66.51 ± 6.73	0.298
		T	65.94 ± 6.79	65.16 ± 6.10	0.646
6	The angle between the vertical plane and the axis of the GPC (°)	F	14.98 ± 6.06	14.31 ± 7.01	0.444
		M	15.26 ± 6.94	14.73 ± 7.97	0.506
		T	15.12 ± 6.50	15.51 ± 7.49	0.308
7	GPF–MS in the coronal plane (mm)	F	14.66 ± 1.20	14.66 ± 1.26	0.991
		M	15.26 ± 1.61	15.32 ± 1.55	0.806
		T	14.97 ± 1.45	14.99 ± 1.45	0.860
8	The distance between the GPF and the occlusal plane of the teeth (mm)	F	18.55 ± 1.79	18.63 ± 1.80	0.169
		M	20.24 ± 2.15	20.38 ± 2.30	0.068
		T	19.40 ± 2.14	19.51 ± 2.24	0.022*
9	TD-GPF (mm)	F	2.98 ± 0.87	3.18 ± 0.72	0.035*
		M	3.56 ± 0.92	3.48 ± 0.82	0.450
		T	3.29 ± 0.94	3.34 ± 0.78	0.446
10	SD-GPF (mm)	F	6.62 ± 1.64	6.26 ± 1.36	0.035*
		M	6.87 ± 1.60	6.40 ± 1.54	0.009*
		T	6.75 ± 1.62	6.34 ± 1.46	0.001*
11	The area of the GPF (mm^2)	F	16.09 ± 7.19	15.81 ± 5.62	0.717
		M	19.44 ± 7.71	17.74 ± 6.32	0.019*
		T	17.87 ± 7.63	16.84 ± 6.06	0.050
12	GPF–MS in the axial plane (mm)	F	13.69 ± 1.24	13.53 ± 1.25	0.220
		M	14.23 ± 1.51	14.24 ± 1.54	0.945
		T	13.96 ± 1.40	13.88 ± 1.44	0.428
13	GPF–PNS (mm)	F	18.30 ± 1.98	17.98 ± 1.83	0.067
		M	19.72 ± 2.59	19.37 ± 2.28	0.036*
		T	19.03 ± 2.41	18.68 ± 2.18	0.005*
14	GPF–IF (mm)	F	31.45 ± 2.26	31.65 ± 2.50	0.466
		M	32.43 ± 2.70	32.70 ± 2.99	0.297
		T	31.95 ± 2.53	32.18 ± 2.80	0.209
15	GPF–PH (mm)	F	11.68 ± 1.68	11.52 ± 1.42	0.623
		M	12.00 ± 1.91	11.02 ± 1.67	0.005*
		T	11.84 ± 1.79	11.28 ± 1.55	0.019 *
16	GPF–AR (mm)	F	2.80 ± 1.24	3.09 ± 1.08	0.219
		M	2.75 ± 1.22	2.69 ± 0.88	0.661
		T	2.77 ± 1.22	2.84 ± 0.97	0.511

G gender, *F* female, *M* male, *T* total, *AR* alveolar ridge, *GPC* greater palatine canal, *GPF* greater palatine foramen, *IF* incisive foramen, *IOF* inferior orbital fissure, *LPC* lesser palatine canal, *MS* midsagittal plane, *PC* pterygoid canal, *PH* pterygoid hamulus, *PNS* posterior nasal spine, *PPF* pterygopalatine fossa, *SD-GPF* the sagittal diameter of the greater palatine foramen, *TD-GPF* the transverse diameter of the greater palatine foramen

*Significant difference

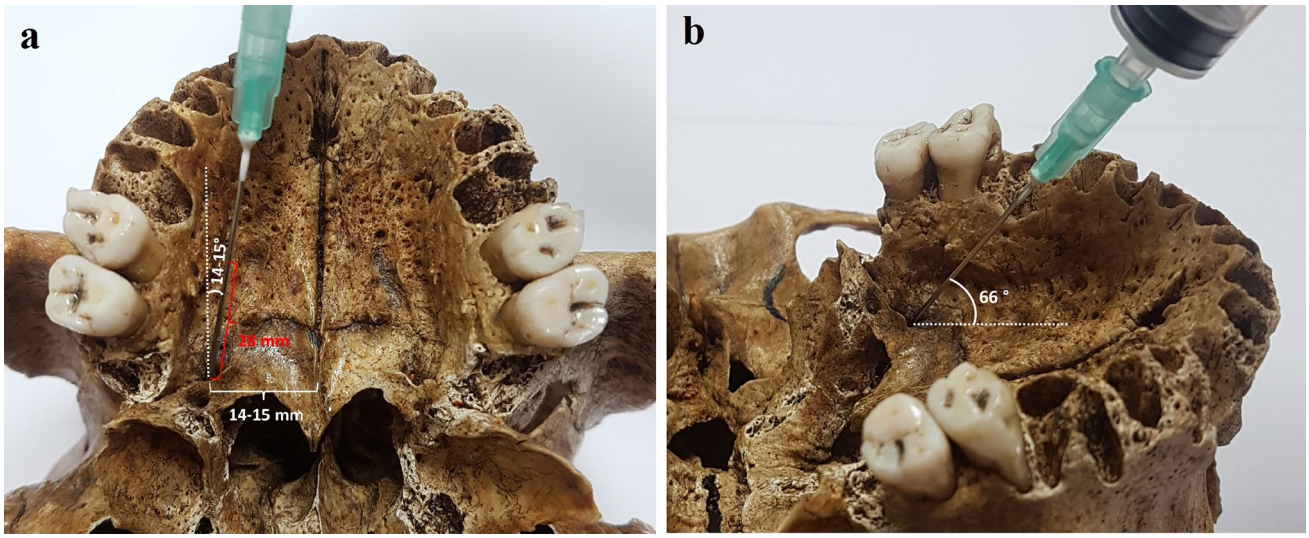

Fig. 9 Recommended localization of the needle for the PPF infiltration. **a** The needle inserted 14–15 mm lateral to the midsagittal plane, the needle pushed forward 28 mm upward at 14°–15° angle on the vertical plane with mediolateral direction, **b** the needle placed at an angle of 66° with anteroposterior direction on the transverse plane, *PPF* pterygopalatine fossa

Table 2 The presence of LPF according to side and gender

Number of LPF	Female		Male	
	Right	Left	Right	Left
1	3 (4.2%)	2 (2.8%)	5 (6.9%)	8 (11.1%)
2	28 (38.9%)	19 (26.4%)	25 (34.2%)	18 (25%)
3	20 (27.8%)	28 (38.9%)	21 (28.8%)	21 (29.2%)
4	20 (27.8%)	22 (30.6%)	19 (26.0%)	18 (25%)
5	1 (1.4%)	1 (1.4%)	3 (4.1%)	7 (9.7%)

LPF lesser palatine foramen

is presented in Table 2. No statistically significant difference was detected by gender and side ($p=0.056$, $p=0.215$ respectively).

The localization of GPF was classified by the posterior margin of the hard palate into three groups: anteriorly, on the same line, posteriorly (Fig. 8; Table 3). The localization of GPF with respect to the maxillary molar teeth is presented in Table 4.

Table 3 Localization of the GPF with respect to the posterior margin of the hard palate

Localization	Right			Left		
	Female	Male	Total	Female	Male	Total
Anteriorly	19 (28.8%)	20 (29.9%)	39 (29.3%)	22 (33.3%)	18 (26.9%)	40 (30.1%)
On the same line	38 (57.6%)	37 (55.2%)	75 (56.4%)	40 (60.6%)	42 (62.7%)	82 (61.7%)
Posteriorly	9 (13.6%)	10 (14.9%)	19 (14.3%)	4 (6.1%)	7 (10.4%)	11 (8.3%)

GPF greater palatine foramen

Table 4 The incidence of the GPF position relative to the maxillary molars

Localization	Right			Left		
	Female	Male	Total	Female	Male	Total
Medial to the 2nd molar	5 (6.66%)	4 (5.33%)	9 (6%)	5 (6.66%)	4 (5.33%)	9 (6%)
Between the 2nd and 3rd molar	17 (22.66%)	14 (18.66%)	31 (20.66%)	16 (21.33%)	15 (10%)	31 (20.66%)
Medial to the 3rd molar	49 (65.33%)	52 (69.33%)	101 (67.33%)	49 (65.33%)	50 (33.3%)	99 (66%)
Behind the 3rd molar	4 (5.33%)	5 (6.66%)	9 (6%)	5 (6.66%)	6 (8%)	11 (7.33%)

GPF greater palatine foramen

Discussion

PPF infiltration is performed to reduce blood flow during endoscopic sinus surgery and septorhinoplasty, as well as to control posterior epistaxis and to provide regional anesthesia in dental procedures [13]. Anesthetic or vasoconstrictor agent administration into the PPF is performed by two different techniques via the sphenopalatine foramen and the GPF. PPF infiltration through the sphenopalatine foramen is generally used in extensive endoscopic surgery, which involves high risks of complication such as nasal epistaxis, nasal tamponade and temporary diplopia. PPF infiltration via GPF is a more effective and safer method [14, 28, 56]. Therefore, this method of obtaining the maxillary nerve block has a high success rate with minimal risk [30].

During the PPF infiltration through the GPC, complications such as intravascular injection, anesthesia of orbital/ocular nerves, infraorbital nerve injury, diplopia, strabismus, insufficient anesthesia, ptosis, positive blood aspiration or trauma of palatine nerves may be observed [13, 32, 47]. The achievement of palatal reconstruction and surgical implant procedures mostly depend on the surgeon's knowledge of the landmarks of the GPF and surrounding structures [7].

During PPF infiltration, if the needle is not advanced sufficiently into the GPC, agent administration will be ineffective. Furthermore, if the needle is advanced too far, the infusion may reach the orbita, which may lead to complications. Therefore, the distance along which the needle should be advanced is important for optimal PPF infiltration. This distance may be determined by measuring the length of the GPC. However, the border between the GPC and the PPF is not always clear; therefore, detection of the superior border of the GPC is not always possible. Defining this border increases the success of the infiltration.

GPF–PC and PC–IOF distances

In many studies, in order to define these distances, GPC and/or PPF has been examined on CT images [3, 5, 11, 18, 37, 38, 43, 49] and CT images of cadavers [13] and dry skulls [33, 51]. However, superior border of the GPC was defined at different levels in these studies. Aoun and Nasseh [3] and Asha et al. [5] determined the superior border of the GPC as the PC and performed their measurements accordingly. Methathrathip et al. [33] measured the total length of GPC and PPF in their study conducted on dry skull. Sheikhi et al. [43] and Tomaszewska et al. [49] suggested that the PC was the superior border of the GPC in the methods; however, they demonstrated the level of IOF in the figure included. Rapado-González et al. [38] did not define the superior border of the GPC in their study investigating the morphology of the GPC; however, they demonstrated it over the PC in the figure. Howard-Swirzinski et al. [18] identified the superior border of the GPC as the PC. The border was demonstrated at the level indicated in the figure in the results, but it was demonstrated at a lower level than the PC in the figure in the methods. Rapado-González et al. [37] defined the superior border of the GPC as the lower limit of the PPF, however, in the figure they showed it to be below the PC. In the following two CT image studies, the border between the GPC and the PPF was not clear. Hwang et al. [19] and cadaveric study of Douglas and Wormald [13] measured the GPC and the PPF lengths; however, they did not mention how they defined the border between these two formations. Das et al. [11] measured the distance from the GPF to the orbital floor in the CT images. Urbano et al. [51] measured the GPC in the dry skull, but did not mention how they define the superior border of GPC (Table 5). Although Hwang et al. [20] stated that CT imaging was the ideal method for the discrimination of the PPF and the GPC, the reason for the difference in determining the superior border of the GPC between most of the studies in the literature is that the border between the PPF and the GPC was not clear. Defining the superior border of the GPC as the IOF will increase the complication of orbital infusion.

Since the superior border of the GPC is not prominent in each case, an accurate measurement of the GPC length is not always possible. If the solution is injected at the level of PC, it will show a favorable effect in the PPF and the risk of complications will be minimized. Therefore, we believe that instead of expressing the length of the GPC for the PPF infiltration, it is more appropriate to express the distance in terms of PC–GPF.

Das et al. [11] recommended advancing the needle 25 mm for the PPF infiltration. Malamed and Trieger [31] suggested this distance as being 32 mm. Stankiewicz [45] reported that the *IOF–GPF* was 40 mm and advancing the needle by 28 mm (25–33 mm) was ideal for PPF infiltration. In the present study, *IOF–GPF* distance was found to be similar to that defined by Stankiewicz [45]. We believe that the ideal level for the PPF infiltration is the PC level, and that the needle should be advanced by 28 mm from the origin of the GPF.

LPC–GPF distance

LPCs locate between GPC and LPF. The LPC starts at a level about 13.26 mm (male: 13.87 mm, female: 12.64 mm) above the GPF. A statistically significant difference was observed between genders ($p = 0.001$).

Table 5 GPF–PC, PC–IOF and GPF–IOF measurements and comparison with the literature

Study	Specimen	Parameter (mm)	Side	Gender	
				Female	Male
Aoun and Nasseh [3]	CT	GPF–PC	R	30.64	
			L	30.60	
Asha et al. [5]	CBCT	GPF–PC	R	26.70 ± 2.34	
			L	27.52 ± 2.40	
Das et al. [11]	CT	GPF–orbital floor	R	37.00 ± 3.00	40.00 ± 2.00
			L		
Douglas and Wormald [13]	CT of cadavers	Length of GPC	N/A	18.50 (17.90–19.10)	
		Length of PPF	N/A	21.60 (20.70–22.50)	
Howard-Swirzinski et al. [18]	CBCT	GPF–PC	N/A	29.00 ± 3.00	
Hwang et al. [20]	CT	Length of GPC	N/A	13.80 ± 2.00	
		Length of PPF	N/A	21.00 ± 3.40	
Methathrathip et al. [33]	Dry skull	Length of GPF and PPF	N/A	28.90 ± 4.00	30.00 ± 4.30
Rapado-González et al. [37]	CBCT	Lover limit of PPF–GPF	R	12.31 ± 1.96	
			L	12.52 ± 2.15	
Sheikhi et al. [43]	CBCT	GPF–PC	R	31.70 ± 2.44	
			L	31.94 ± 2.40	
Tomaszewska et al. [49]	CBCT	GPF–PC	R	29.60 ± 2.50	32.60 ± 2.80
			L	29.90 ± 2.70	32.40 ± 2.80
Urbano et al. [51]	Dry skull	Length of GPC	N/A	36.40	35.30
Present Study	CBCT	GPF–CP	R	27.48 ± 3.10	29.27 ± 3.59
			L	26.71 ± 2.82	29.33 ± 3.14
		CP–IOF	R	8.34 ± 2.51	9.55 ± 2.93
			L	8.68 ± 2.43	9.42 ± 2.43

R right, *L* left, *N/A* non available, *GPF* greater palatine foramen, *IOF* inferior orbital fissure, *PC* pterygoid canal

The angle between the axis of the GPC and the axis of the PPF

In this study, this angle was found to be 150.03° ± 9.27°, which is close to the 159.80° ± 7.10° observed by Hwang et al. [20]. No significant difference was observed between genders in both studies ($p = 0.192$ and $p = 0.074$, respectively). This angle was close to 180°. Hwang et al. [20] state that when attempting to advance the needle to infiltrate the PPF through the GPF, an excessive injection may lead to penetration to the orbital cavity through the IOF without resistance.

TP–GPC and VP–GPC angles

For PPF infiltration, the studies in which the angle defined in transverse plane, Stankiewicz [45] and Das et al. [11] recommended advancing the needle at 45° and 60°, respectively. The angle between the hard palate and the axis of GPC is defined to be 67.40° ± 6.90° by Hwang et al. [20], 45.88° (37.00°–57.50°) by Malamed and Trieger [31], and 57.90° ± 5.80° by Methathrathip [33]. In this study, *TP–GPC* was found to be 66.05°. *VP–GPC* was defined as 6.70° ± 5.20° by Methathrathip [33], and as 6° (2°–10°) by Nimigean et al. [35]. In this study, it was found to be 14.82°. We believe that for a successful infiltration, the needle should be inserted into the GPF at angle of 66° on the transverse plane and 14°–15° on the vertical plane.

GPF–MS, GPF–PNS, GPF–IF and GPF–PH distances

GPF–MS is a significant landmark for a number of procedures such as restorative approaches and palatal implant surgery [7]. There are many studies that have investigated this distance, and except Suzuki et al. [46], all have found similar results (Table 6) [1, 2, 7, 9, 10, 12, 20–27, 29, 33, 35–37, 39, 40, 42, 48–52, 54, 55]. In this study, *GPF–MS* was measured at the coronal and the axial planes, and both results were similar (14.98 ± 1.45 mm, 13.92 ± 0.86 mm, respectively). A significant difference was found between genders ($p = 0.001$). This demonstrates that the palatal width in the female is smaller than that in the male. Methathrathip et al. [33] stated that PNS was an easily identifiable structure without consideration for the edentulous or dentulous cases. According to Hwang et al. [20] the location of the GPF might be determined relative to the PNS. In contrast,

Table 6 GPF–MS, TD-GPF, SD-GPF, GPF–PNS, GPF–IF measurements and comparison with the literature

Study	Specimen	*n*	Side	GPF–MS (mm)	TD-GPF (mm)	SD-GPF (mm)	GPF–PNS (mm)	GPF–IF (mm)
Ajmani [1]	Dry skull[a]	34	R	14.70 ± 0.96				
			L	14.60 ± 1.08				
	Dry skull[b]	65	R	15.40 ± 0.21				
			L	15.40 ± 0.21				
Anjankar et al. [2]	Dry skull	86	R	15.40				36.20
			L	15.100				35.70
Aoun et al. [4]	CBCT	79	R		6.39 ± 1.28			
			L		6.42 ± 1.09			
Cagimni et al. [7]	Dry skull	120	R	16.25 ± 1.60	5.30 ± 0.90	5.30 ± 0.90		40.63 ± 3.81
			L	16.06 ± 1.62	5.40 ± 0.90	5.40 ± 0.90		40.57 ± 3.63
Chrcanovic and Custódio [9]	Dry skull	80	R	14.68 ± 1.56				36.21 ± 3.16
			L	14.44 ± 1.43				36.52 ± 3.34
D'Souza et al. [10]	Dry skull	40	R	14.60 ± 1.47				
			L	14.40 ± 1.40				
Dave et al. [12]	Dry skull	100	R	M: 16.70 ± 0.11 F: 16.20 ± 0.11				
			L	M: 16.60 ± 0.11 F: 16.40 ± 0.11				
Hwang et al. [20]	HRCT	50	N/A	16.20 ± 1.30	4.50 ± 0.70	2.20 ± 0.40		
Ikuta et al. [21]	CBCT	50	N/A	15.20 ± 1.45	3.10 ± 0.47	3.10 ± 0.47		
Jaffar and Hamadah [22]	Dry skull	50	N/A	15.71 ± 1.36	4.60 ± 0.98	2.77 ± 0.63		
Jotania et al. [23]	Dry skull	60	R	14.80 ± 1.20				
			L	14.83 ± 1.52				
Kang et al. [24]	CT	107	N/A	16.32 ± 1.32				32.04 ± 3.31
Klosek and Rungruang [25]	Cadaver	41	N/A	14.70 ± 3.30	F: 5.07 ± 0.95 M: 4.90 ± 8.30	F: 2.77 ± 0.80 M: 2.60 ± 8.30		34.00 ± 7.30
Kumar et al. [26]	Dry skull	100	R	14.30 ± 1.42				36.60 ± 2.20
			L	14.40 ± 1.27				35.70 ± 3.94
Langenegger et al. [27]	Dry skull	100	R	15.10 ± 2.60	2.50 ± 0.50[c]			
			L	14.90 ± 1.80				
Lopes et al. [29]	Dry skull	94	R	15.60 ± 1.30				
			L	15.40 ± 1.40				
Methathrathip et al. [33]	Dry skull	105	N/A	16.20 ± 1.30	4.90 ± 0.90	2.70 ± 0.50		
Moreira et al. [34]	Dry skull	135[d]	R				Adult: 17.70 ± 0.31 Aged: 17.58 ± 0.39	Adult: 41.35 ± 0.58 Aged: 41.35 ± 1.09
			L				Adult: 17.55 ± 0.29 Aged: 17.33 ± 0.42	Adult: 41.43 ± 0.58 Aged: 41.72 ± 1.00
Nimigean et al. [35]	Dry skull	100	N/A	14.50 ± 0.80	4.90 ± 0.90	3.00 ± 0.50		
Piagkou et al. [36]	Dry skull	71	R	15.30 ± 1.30	5.30 ± 0.90	2.60 ± 0.60		
			L		5.40 ± 0.90	2.70 ± 0.50		
Rapado-González et al. [37]	CBCT	150	R	15.05 ± 2.00	6.04 ± 1.18	2.72 ± 0.74		
			L	15.44 ± 1.98	6.04 ± 1.12	2.64 ± 0.75		
Renu [39]	Dry skull	100	R	15.30				
			L	15.00				

Table 6 (continued)

Study	Specimen	*n*	Side	GPF–MS (mm)	TD-GPF (mm)	SD-GPF (mm)	GPF–PNS (mm)	GPF–IF (mm)
Saralaya and Nayak [40]	Dry skull	132	R	14.70 ± 1.55				37.20 ± 2.92
			L	14.70 ± 1.46				37.40 ± 3.01
Sharma and Garud [42]	Dry skull	100	R	14.71 ± 1.38		4.67 ± 1.13		35.42 ± 2.75
			L	14.41 ± 1.39		4.88 ± 1.58		35.66 ± 2.61
Suzuki et al. [46]	Dry skull	20	N/A	29.80 ± 1.10	3.96	2.72		
Teixeira et al. [48]	Dry skull	141	R	15.70 ± 1.60				39.30 ± 3.40
			L	16.20 ± 1.60				39.10 ± 3.80
Tomaszewska et al. [49]	CT	1500	R		F: 5.00 ± 0.40 M: 5.10 ± 0.50	F: 2.80 ± 0.80 M: 3.00 ± 0.70		
			L		F: 5.00 ± 0.40 M: 5.10 ± 0.40	F: 2.80 ± 0.80 M: 2.90 ± 0.50		
Tomaszewska et al. [50]	CT + Dry skull	1200 + 150	R	16.10 ± 1.50	5.10 ± 0.50	3.00 ± 0.80	17.00 ± 1.40	34.00 ± 3.00
			L	15.60 ± 1.50			17.00 ± 1.50	34.30 ± 3.10
Urbano et al. [51]	Dry skull	43	R	16.63				
			L	16.39				
Vinay et al. [52]	Dry skull	150	R	14.80 ± 0.16				36.60 ± 2.20
			L	14.80 ± 0.15				35.90 ± 3.94
Wang et al. [54]	Dry skull	100	R	15.95 ± 0.15				
			L	16.01 ± 0.14				
Westmoreland and Blanton [55]	Dry skull	300	R	14.80 ± 0.07				
			L	15.00 ± 0.07				
Present Study	CBCT	150	R	Coronal: 14.97 ± 1.45 Axial: 13.96 ± 1.40	3.29 ± 0.94	6.75 ± 1.62	19.03 ± 2.41	31.95 ± 2.53
			L	Coronal: 14.99 ± 1.45 Axial: 13.88 ± 1.44	3.34 ± 0.78	6.34 ± 1.46	18.68 ± 2.18	32.18 ± 2.80

F female, *M* male, *R* right, *L* left, *N/A* not available, *GPF* greater palatine foramen, *IF* incisive foramen, *MS* midsagittal plane, *PNS* posterior nasal spine, *SD-GPF* the sagittal diameter of the greater palatine foramen, *TD-GPF* the transverse diameter of the greater palatine foramen

[a]Indian

[b]Nigerian

[c]Least diameter of foramens

[d]Adult and aged

Kang et al. [24] stated that the PNS was difficult to identify; for these reasons, using *GPF–PNS* as a reference value for anesthesia may be difficult. In this study, *GPF–PNS* was found to be 18.86 mm, which is consistent with the literature (Table 6) [34, 50]. *GPF–IF* is significant to estimate the possible length of the graft, which is used for the restoration of the bony palate following a traumatic injury or a tumor surgery [7]. In previous studies [2, 7, 9, 24–26, 34, 40, 42, 48, 50, 52], *GPF–IF* was reported in a range of 34.00–41.35 mm (Table 6). In this study, *GPF–IF* was found to be 31.45 mm in female and 32.43 mm in male ($p = 0.105$). According to Nimigean et al. [35], *GPF–PH* is an important landmark, because the PH is palpable on the posterolateral side of the soft palate. In this study, *GPF–PH* was found to be 11.56 ± 1.67 mm, which is consistent with the literature (Table 7) [27, 31, 35, 42, 50].

SD-GPF and TD-GPF diameters

In previous studies, *SD-GPF* was reported in a range of 2.20–5.40 mm and *TD-GPF* was reported in a range of 3.10–6.42 mm (Table 6) [4, 7, 20–22, 25, 27, 33, 35–37, 42, 46, 49, 50]. In this study, *SD-GPF* was observed to be 6.44 mm in females and 6.64 mm in males, and no significant difference was observed between genders ($p = 0.298$). *TD-GPF* was found to be 3.08 mm in females and 3.52 mm in males. A significant difference was found between genders in *TD-GPF* ($p = 0.001$).

Table 7 GPF–PH measurement and comparison with the literature

Study	Specimen	*n*	Side	GPF–PH (mm)
Langenegger et al. [27]	Dry skull	100	R	12.60 ± 1.90
			L	12.30 ± 1.80
Malamed and Trieger [31]	Dry skull	204	N/A	12.00 (3.00–20.00)
Nimigean et al. [35]	Dry skull	100	N/A	12.00 ± 1.80
Sharma and Garud [42]	Dry skull	100	R	12.12 ± 2.53
			L	11.47 ± 1.90
Tomaszewska et al. [50]	CT + dry skull	1350	R	11.90 ± 1.00
			L	12.00 ± 1.10
Present study	CBCT	150	R	11.84 ± 1.79
			L	11.28 ± 1.55

R right, *L* left, *N/A* not available, *GPF* greater palatine foramen, *PH* pterygoid hamulus

The distance between the GPF and the occlusal plane of the teeth

Kang et al. [24] defined this distance as 22.13 ± 3.36 mm. Similar to Kang et al. [24], it was observed to be 19.45 ± 2.19 mm in this study. We believe that this measurement can be used as a reference value to determine the localization of the GPF.

The area of the GPF

According to Benninger et al. [6], the mucosa covering the area of the GPF is a donor site for soft tissue grafts. Gupta et al. [16] report that adenoid cystic carcinoma is most commonly found in the area of the GPF of the palate. Although it is significant for these reasons, there is no study in the literature measuring the area of the GPF. In this study, it was found to be 17.35 ± 6.90 mm^2.

GPF–AR distance

As for the measurement of *GPF–AR*, in previous studies [7, 21, 33, 36, 50] this distance was reported in a range of 2.90–13.80 mm (Table 8). In this study, it was found to be 2.81 mm. *GPF–AR* is used in performing several clinical operations such as implant-assisted dental reconstruction, regional anesthesia and preservation of the palatine nerves during surgical procedures [7].

The number of the LPF

Although Hassanali and Mwaniki [17] reported that there was no study in the literature reporting any significance of having a single or multiple LPF, the number of LPF has been investigated in many studies [7, 10, 17, 22, 23, 26, 36, 38, 40, 42, 50] (Table 9). In previous studies, the number of LPF ranges from 0 to 5. They have mostly reported one or two LPFs. However, in this study, LPFs were frequently found to be two or three in number. Absence of LPF was not observed in the present study.

The localization of the GPF with respect to the posterior margin of the palatine bone

The localization of the GPF relative to the posterior margin of the palatine bone is significant in prosthetic dentistry [7].

Table 8 GPF–AR measurement and comparison with the literature

Study	Specimen	*n*	Side	GPF–AR (mm)
Cagimni et al. [7]	Dry skull	120	R	4.06 ± 0.30
			L	4.06 ± 0.36
Ikuta et al. [21]	CBCT	50	N/A	7.90 ± 2.04
Methathrathip et al. [33]	Dry skull	105	N/A	13.80 ± 2.40
Piagkou et al. [36]	Dry skull	71	R	3.10 ± 1.70
			L	2.90 ± 1.60
Tomaszewska et al. [50]	CT + Dry skull	1200 + 150	R	3.00 ± 1.30
			L	2.90 ± 1.30
Present Study	CBCT	150	R	2.77 ± 1.22
			L	2.84 ± 0.97

R right, *L* left, *N/A* not available, *AR* alveolar ridge, *GPF* greater palatine foramen

Table 9 Evaluation of the LPF numbers and comparison with the literature

Study	Specimen	*n*	Side	Number of LPF					
				0	1	2	3	4	5
Cagimni et al. [7]	Dry skull	120	R	3 (2.5%)	49 (41%)	40 (33%)	21 (17.5%)	5 (4%)	2 (2%)
			L	3 (2.5%)	47 (39.2%)	49 (40.8%)	14 (11.7%)	4 (3.3%)	3 (2.5%)
D'Souza et al. [10]	Dry skull	40	N/A		62.5%	30%	7.5%		
Hassanali and Mwaniki [17]	Dry skull	125	R		51.20%	38.20%	8.90%	1.60%	0.00%
			L		51.20%	33.60%	8.40%	5.00%	0.84%
Jaffar and Hamadah [22]	Dry skull	50	N/A	4.0%	41.0%	55.0%			
Jotania et al. [23]	Dry skull	60	N/A	0.83%	48.34%	38.33%	10.83%	1.67%	
Piagkou et al. [36]	Dry skull	71	R		35 (49.2%)	22 (31%)	10 (14.1%)	3 (4.2%)	1 (1.4%)
			L		41 (57.7%)	22 (31%)	5 (7%)	1 (1.4%)	2 (2.8%)
Kumar et al. [26]	Dry skull	100	R	1.20 ± 0.53					
			L	1.30 ± 0.53					
Saralaya and Nayak [40]	Dry skull	132	R	1.80 ± 0.80					
			L	1.90 ± 0.89					
Sharma and Garud [42]	Dry skull	100	R	1.39 (0–5)					
			L	1.43 (0–5)					
Tomaszewska et al. [50]	CT + dry skull	1200 + 150	R	1.60 (0–5)					
			L	1.50 (0–5)					
Present Study	CBCT	150	R	0	8 (5.5%)	53 (36.6%)	41 (28.3%)	39 (26.9%)	4 (2.8%)
			L	0	10 (7.0%)	37 (25.7%)	49 (34%)	40 (27.8%)	8 (5.6%)

R right, *L* left, *N/A* not available, *LPF* lesser palatine foramen

According to the data obtained in this study, the GPF was on the same line of the posterior margin of the hard palate in more than half of the cases. Knowing the localization of the GPF, with respect to the posterior margin of the palate, would increase success during interventions.

The localization of the GPF according to the maxillary molar teeth

The GPF is located at the level of the maxillary molar teeth, and knowing this relation would contribute to the success of the procedure. Tomaszewska et al. [50] stated that the maxillary molar teeth were the best landmarks for locating the GPF. The results obtained in this study were in compliance with the findings observed in the literature [1, 2, 5, 7, 9, 10, 12, 15, 17, 21–23, 25–27, 31, 33, 35, 36, 39–42, 50, 52, 54, 55], and the GPF was most commonly located at the level of the third molar teeth (Table 10). Third molar teeth can be easily located by visualization. Methathrathip et al. [33] stated that when the third maxillary molar teeth are absent, their location can be estimated accurately by using their relation to the other maxillary molars.

Conclusion

Our results may help to insert to needle properly for application of maxillary nerve block with a high success rate and minimal complication. We recommend that the needle should be inserted 14–15 mm lateral to the midsagittal plane, 19–20 mm over the occlusal plane of the teeth and on the same line as the third molar teeth. For PPF infiltration through the GPF, the needle should be pushed forward 28 mm upward at 66° angle on the transverse plane and 14°–15° angle on the vertical plane (Fig. 9). We believe that the present study would help to prevent the complication of surgical interferences and restoration procedures, as the results may enable the clinicians to prepare before surgical procedures. Moreover, the results obtained in this study have contributed to the literature.

Table 10 Literature comparison of the localization of GPF with respect to the maxillary molar teeth

Study	Specimen	*n*	Side	Between the 1st and 2nd molar	Medial to the 2nd molar	Between the 2nd and 3rd molar	Medial to the 3rd molar	Behind the 3rd molar
Ajmani [1]	Dry skull[a]	34	R			10	23	1
			L			12	21	1
Ajmani [1]	Dry skull[b]	65	R		7	24	34	
			L		10	26	29	
Anjankar et al. [2]	Dry skull	86	N/A		6 (6.98%)	14 (16.27%)	63 (73.26%)	3 (3.49%)
Asha et al. [5]	CBCT	100	N/A		Medial surface of the 2nd molar: 16%, middle of the 2nd molar and its distal surface: 34%		Medial face of the 3rd molar and its center: 25% Middle of the 3rd molar and its distal surface: 18%	7%
Cagimni et al. [7]	Dry skull	120	R		1%		Between proximal surface of the 3rd molar: 32% Between distal surface of the 3rd molar: 46%	21%
			L		2.5%		Between proximal surface of the 3rd molar: 37.5% Between distal surface of the 3rd molar: 37.5%	22.5%
Chrcanovic and Custódio [9]	Dry skull	80	N/A			6.19%	54.87%	38.94%
D'Souza et al. [10]	Dry skull	40	R		1 (2.5%)	9 (22.5%)	30 (75%)	
			L		1 (2.5%)	10 (25%)	29 (72.5%)	
Dave et al. [12]	Dry skull	100	N/A		2 (1%)	7 (3.5%)	175 (87.5%)	16 (8%)
Fu et al. [15]	Cadaver	11	N/A		19.1%	66.6%	14.3%	
Hassanali and Mwaniki [17]	Dry skull	125	N/A		10.4%	13.6%	76.0%	
Ikuta et al. [21]	CBCT	50	N/A		3%		Between the middle of the 3rd molar and its distal face: 39% Between the medial face of the 3rd molar and its center: 53%	5%
Jaffar and Hamadah [22]	Dry skull	50	N/A		12.0%	19.0%	55.0%	14.0%
Jotania et al. [23]	Dry skull	60	N/A		4.17%	17.50%	78.33%	
Klosek ve Rungruang [25]	Cadaver	41	N/A	F: 14.3%, M: 0	F: 35.7%, M: 65%	F: 35.7%, M: 10%	F: 14.3%, M: 25%	
Kumar et al. [26]	Dry skull	100	R		5 (5%)	9 (9%)	85 (85%)	1 (1%)
			L		5 (5%)	9 (9%)	85 (85%)	1 (1%)

Table 10 (continued)

Study	Specimen	*n*	Side	Between the 1st and 2nd molar	Medial to the 2nd molar	Between the 2nd and 3rd molar	Medial to the 3rd molar	Behind the 3rd molar
Langenegger et al. [27]	Dry skull	100	R		0	0	71 (71%)	39 (39%)
			L		1 (1%)	1 (1%)	64 (64%)	34 (34%)
Malamed and Trieger [31]	Dry skull	204	N/A		63 (39.87%)		Anterior half of 3rd molar: 80 (50.63%) Posterior half of 3rd molar: 15 (9.49%)	
Methathrathip et al. [33]	Dry skull	105	N/A		9 (5.6%)	37 (23.1%)	103 (64.4%)	11 (6.9%)
Nimigean et al. [35]	Dry skull	100	N/A		9 (9%)	15 (15%)	73 (73%)	3 (3%)
Piagkou et al. [36]	Dry skull	71	R		9 (16.6%)		41 (76.9%)	4 (7.4%)
			L		9 (17%)		40 (75.5%)	4 (7.5%)
Renu [39]	Dry skull	100	R		9	23	50	18
			L		9	28	45	18
Saralaya and Nayak [40]	Dry skull	132	R		1 (0.8%)	33 (25%)	97 (73.5%)	1 (0.8%)
			L		0	31 (23.5%)	100 (75.8%)	1 (0.8%)
Sarilita et al. [41]	Dry skull	65	N/A		4.0%	37.3%	58.7%	
Sharma and Garud [42]	Dry skull	100	R		Posterior half of 2nd molar: 6 (8.70%)		Anterior half of 3rd molar: 23 (33.33%) Posterior half of 3rd molar: 25 (36.23%)	10 (14.29%)
			L		Anterior half of 2nd molar: 1 (1.43%) Posterior half of 2nd molar: 5 (7.14%)		Anterior half of 3rd molar: 26 (37.14%) Posterior half of 3rd molar: 28 (40%)	15 (21.74%)
Tomaszewska et al. [50]	CT + Dry skull	1200 + 150	R		15.5%	6.8%	75.4%	1.1%
			L		17.1%	6.8%	74.0%	1.1%
Vinay et al. [52]	Dry skull	150	R		5 (3.33%)	28 (18.67%)	115 (76.67%)	2 (1.33%)
			L		6 (4%)	29 (19.33%)	113 (75.34%)	2 (1.33%)
Wang et al. [54]	Dry skull	100	R	0	14%	46%	40%	0
			L	2%	20%	51%	27%	0
Westmoreland and Blanton [55]	Dry skull	300	R		26	104	152	18
			L		32	98	152	18
Present Study	CBCT	150	R		9 (6%)	31 (20.66%)	101 (67.33%)	9 (6%)
			L		9 (6%)	31 (20.66%)	99 (66%)	11 (7.33%)

R right, *L* left, *N/A* not available, *GPF* greater palatine foramen

[a]Indian

[b]Nigeria

Acknowledgements The authors are greatful to Associate Professor Dr. Seval KUL, Department of Biostatistics, School of Medicine, Gaziantep University, for the support.

Author contributions BI: protocol/project development, data collection or management, data analysis and manuscript writing/editing. OM: data collection or management, data analysis and manuscript writing/editing. KP: data analysis and manuscript writing/editing. YED: manuscript writing/editing.

Compliance with ethical standards

Conflict of interest The authors declare that they have no conflict of interest.

Ethical standards This study was approved by the ethics committee of Gaziantep University (approval date and number: 07 March 2016; 2016/72). We declare that this human study has been approved by the ethics committee of Gaziantep University and has, therefore, been performed in accordance with the ethical standards laid down in the Declaration of Helsinki and its later amendments.

References

1. Ajmani M (1994) Anatomical variation in position of the greater palatine foramen in the adult human skull. J Anat 184:635–637
2. Anjankar VP, Gupta S, Nair S, Thaduri N, Trivedi G, Budhiraja V (2014) Analysis of position of greater palatine foramen in central Indian adult skulls: a consideration for maxillary nerve block. Indian J Pharmaceut Biol Res 2(1):51–54
3. Aoun G, Nasseh I (2016) The Length of the Greater Palatine Canal in a Lebanese Population: a Radio-anatomical Study. Acta Inform Med 24(6):397–400. https://doi.org/10.5455/aim.2016.24.397-400
4. Aoun G, Nasseh I, Sokhn S (2016) Radio-anatomical study of the greater palatine canal and the pterygopalatine fossa in a Lebanese population: a consideration for maxillary nerve block. J Clin Imaging Sci 6(3):1–7. https://doi.org/10.4103/2156-7514.190862
5. Asha M, Kumar GA, Anupama VS, Jigna VR, Diksha M (2015) Cone Beam Computed Tomographic Analysis of Anatomical Variations of Greater Palatine Canal and Foramen in Relation to Gender in South Indian Population. Oral Health Dent Manag 14:384–390
6. Benninger B, Andrews K, Carter W (2012) Clinical measurements of hard palate and implications for subepithelial connective tissue grafts with suggestions for palatal nomenclature. J Oral Maxillofac Surg 70:149–153. https://doi.org/10.1016/j.joms.2011.03.066
7. Cagimni P, Govsa F, Ozer MA, Kazak Z (2016) Computerized analysis of the greater palatine foramen to gain the palatine neurovascular bundle during palatal surgery. Surg Radiol Anat 39(2):177–184. https://doi.org/10.1007/s00276-016-1691-0
8. Chen CC, Chen ZX, Yang XD, Zhengg ZW, Li ZP, Huang F, Kon F-Z, Zhang C-s (2010) Comparative research of the thin transverse sectional anatomy and the multislice spiral CT on pterygopalatine fossa. Turk Neurosurg 20(2):151–158
9. Chrcanovic BR, Custódio AL (2010) Anatomical variation in the position of the greater palatine foramen. J Oral Sci 52:109–113
10. D'Souza AS, Mamatha H, Jyothi N (2012) Morphometric analysis of hard palate in south Indian skulls. Biomed Res 23:173–175
11. Das S, Kim D, Cannon TY, Ebert CS, Senior BA (2006) High-resolution computed tomography analysis of the greater palatine canal. Am J Rhinol Allergy 20:603–608
12. Dave MR, Yagain VK, Anadkat S (2013) A study of the anatomical variations in the position of the greater palatine foramen in adult human skulls and its clinical significance. Int J Morphol 31:578–583
13. Douglas R, Wormald PJ (2006) Pterygopalatine fossa infiltration through the greater palatine foramen: where to bend the needle. Laryngoscope 116:1255–1257. https://doi.org/10.1097/01.mlg.0000226005.43817.a2
14. Felisati G, Arnone F, Lozza P, Leone M, Curone M, Bussone G (2006) Sphenopalatine endoscopic ganglion block: a revision of a traditional technique for cluster headache. Laryngoscope 116:1447–1450. https://doi.org/10.1097/01.mlg.0000227997.48020.44
15. Fu J-H, Hasso DG, Yeh C-Y, Leong DJ, Chan H-L, Wang H-L (2011) The accuracy of identifying the greater palatine neurovascular bundle: a cadaver study. J Periodontol 82:1000–1006. https://doi.org/10.1902/jop.2011.100619
16. Gupta A, Gowri V, Sunil V, Shah G, Jain A, Thomas H (2015) Adenoid cystic carcinoma of palate: a case report. Adv Human Biol 5:93–96
17. Hassanali J, Mwaniki D (1984) Palatal analysis and osteology of the hard palate of the Kenyan African skulls. Anat Rec 209:273–280
18. Howard-Swirzinski K, Edwards PC, Saini TS, Norton NS (2010) Length and geometric patterns of the greater palatine canal observed in cone beam computed tomography. Int J Dent. https://doi.org/10.1155/2010/292753
19. Hwang SH, Joo YH, Seo JH, Kim SW, Cho JH, Kang JM (2011) Three-dimensional computed tomography analysis to help define an endoscopic endonasal approach of the pterygopalatine fossa. Am J Rhinol Allergy 25:346–350
20. Hwang SH, Seo JH, Joo YH, Kim BG, Cho JH, Kang JM (2011) An anatomic study using three-dimensional reconstruction for pterygopalatine fossa infiltration via the greater palatine canal. Clin Anat 24:576–582
21. Ikuta CRS, Cardoso CL, Ferreira-Júnior O, Lauris JRP, Souza PHC, Rubira-Bullen IRF (2013) Position of the greater palatine foramen: an anatomical study through cone beam computed tomography images. Surg Radiol Anat 35:837–842
22. Jaffar AA, Hamadah HJ (2003) An analysis of the position of the greater palatine foramen. J Basic Med Sci 3:24–32
23. Jotania B, Patel S, Patel S, Patel P, Patel S, Patel K (2013) Morphometric analysis of hard palate. Int J Res Med 2:72–75
24. Kang S-H, Byun I-Y, Kim J-H, Park H-K, Kim M-K (2012) Three-dimensional analysis of maxillary anatomic landmarks for greater palatine nerve block anesthesia. J Craniofac Surg 23:e199–e202
25. Klosek SK, Rungruang T (2009) Anatomical study of the greater palatine artery and related structures of the palatal vault: considerations for palate as the subepithelial connective tissue graft donor site. Surg Radiol Anat 31:245–250
26. Kumar A, Sharma A, Singh P (2011) Assessment of the relative location of greater palatine foramen in adult Indian skulls: consideration for maxillary nerve block. Eur J Anat 15:150–154
27. Langenegger J, Lownie J, Cleaton-Jones P (1983) The relationship of the greater palatine foramen to the molar teeth and pterygoid hamulus in human skulls. J Dent 11:249–256
28. Lee WC, Kapur TR, Ramsden WN (1997) Local and regional anesthesia for functional endoscopic sinus surgery. Ann Otol Rhinol Laryngol 106:767–769
29. Lopes P, Santos A, Pereira G, Oliveira V (2011) Morphometric analysis of the greater palatine foramen in dry Southern Brazilian adult skulls. Int J Morphol 29:420–423
30. Malamed SF (2014) Handbook of local anesthesia. Elsevier Health Sciences
31. Malamed SF, Trieger N (1983) Intraoral maxillary nerve block: an anatomical and clinical study. Anesth Prog 30:44–48
32. Mercuri LG (1979) Intraoral second division nerve block. Oral Surg Oral Med Oral Pathol 47:109–113
33. Methathrathip D, Apinhasmit W, Chompoopong S, Lertsirithong A, Ariyawatkul T, Sangvichien S (2005) Anatomy of greater palatine foramen and canal and pterygopalatine fossa in Thais: considerations for maxillary nerve block. Surg Radiol Anat 27:511–516
34. Moreira R, Sgrott E, Stuker H, Alonso L, Smith R (2008) Palatal asymmetry during development: an anatomical study. Clin Anat 21:398–404. https://doi.org/10.1002/ca.20638

35. Nimigean V, Nimigean VR, Buţincu L, Sălăvăstru D, Podoleanu L (2013) Anatomical and clinical considerations regarding the greater palatine foramen. Rom J Morphol Embryol 54:779–783
36. Piagkou M, Xanthos T, Anagnostopoulou S, Demesticha T, Kotsiomitis E, Piagkos G, Protogerou V, Lappas D, Skandalakis P, Johnson EO (2012) Anatomical variation and morphology in the position of the palatine foramina in adult human skulls from Greece. J Craniomaxillofac Surg 40:e206–e210
37. Rapado-González O, Suárez-Quintanilla J, Otero-Cepeda X, Fernández-Alonso A, Suárez-Cunqueiro M (2015) Morphometric study of the greater palatine canal: cone-beam computed tomography. Surg Radiol Anat 37:1217–1224
38. Rapado-González O, Suárez-Quintanilla J, Suárez-Cunqueiro MM (2017) Anatomical variations of the greater palatine canal in cone-beam computed tomography. Surg Radiol Anat 39(7):717–723. https://doi.org/10.1007/s00276-016-1791-x
39. Renu C (2013) The position of greater palatine foramen in the adult human skulls of North Indian origin. J Surg Acad 3:54–57
40. Saralaya V, Nayak S (2007) The relative position of the greater palatine foramen in dry Indian skulls. Singapore Med J 48(12):1143–1146
41. Sarilita E, Soames R (2015) Morphology of the hard palate: A study of dry skulls and review of the literature. Rev Arg de Anat Clin 7:34–43
42. Sharma NA, Garud RS (2013) Greater palatine foramen—key to successful hemimaxillary anaesthesia: a morphometric study and report of a rare aberration. Singapore Med J 54:152–159
43. Sheikhi M, Zamaninaser A, Jalalian F (2013) Length and anatomic routes of the greater palatine canal as observedby cone beam computed tomography. Dent Res J (Isfahan) 10(2):155–161
44. Standring S (2016) Gray's anatomy: the anatomical basis of clinical practice. Elsevier
45. Stankiewicz JA (1988) Greater palatine foramen injection made easy. Laryngoscope 98:580–581. https://doi.org/10.1288/00005537-198805000-00022
46. Suzuki M, Omine Y, Shimoo Y, Yamamoto M, Kaketa A, Kasahara M, Serikawa M, Rhee S, Matsubayashi T, Matsunaga S (2016) Regional anatomical observation of morphology of greater palatine canal and surrounding structures. Bull Tokyo Dent Coll 57(4):223–231
47. Sved AM, Wong JD, Donkor P, Horan J, Rix L, Curtin J, Vickers R (1992) Complications associated with maxillary nerve block anaesthesia via the greater palatine canal. Aust Dent J 37(5):340–345
48. Teixeira C, Souza V, Marques C, Silva Junior W, Pereira K (2010) Topography of the greater palatine foramen in macerated skulls. J Morphol Sci 27:88–92
49. Tomaszewska IM, Kmiotek EK, Pena IZ, Średniawa M, Czyżowska K, Chrzan R, Nowakowski M, Walocha JA (2015) Computed tomography morphometric analysis of the greater palatine canal: A study of 1,500 head CT scans and a systematic review of literature. Anat Sci Int 90(4):287–297
50. Tomaszewska IM, Tomaszewski KA, Kmiotek EK, Pena IZ, Urbanik A, Nowakowski M, Walocha JA (2014) Anatomical landmarks for the localization of the greater palatine foramen—a study of 1200 head CTs, 150 dry skulls, systematic review of literature and meta-analysis. J Anat 225:419–435. https://doi.org/10.1111/joa.12221
51. Urbano E, Melo K, Costa S (2010) Morphologic study of the greater palatine canal. J Morphol Sci 27:102–104
52. Vinay K, Beena D, Vishal K (2012) Morphometric analysis of the greater palatine foramen in south Indian adult skulls. Int J Basic Appl Med Sci 2:5–8
53. von Arx T, Lozanoff S (2017) Pterygopalatine Fossa. In: Clinical oral anatomy. Springer, pp 251–270
54. Wang T, Kuo K, Shih C, Ho L, Liu J (1988) Assessment of the relative locations of the greater palatine foramen in adult Chinese skulls. Acta Anat (Basel) 132:182–186
55. Westmoreland EE, Blanton PL (1982) An analysis of the variations in position of the greater palatine foramen in the adult human skull. Anat Rec 204:383–388
56. Wormald P-J (2012) Endoscopic sinus surgery: anatomy, three-dimensional reconstruction, and surgical technique. Thieme
57. Wormald P-J, Athanasiadis T, Rees G, Robinson S (2005) An evaluation of effect of pterygopalatine fossa injection with local anesthetic and adrenalin in the control of nasal bleeding during endoscopic sinus surgery. Am J Rhinol 19:288–292